Influence of Rare Earth (La, Pr, Nd, Gd, and Sm) Metals on the Methane Decomposition Activity of Ni−Al Catalysts

Chatla Anjaneyulu,[†] Gutta Naresh,[‡] Velisoju Vijay Kumar,[‡] James Tardio,[‡] Tumula Venkateshwar Rao,[†] and Akula Venugopal*[,†,‡]

[†]Inorganic & Physical Chemistry Division, CSIR-Indian Institute of Chemical Technology, Tarnaka, Hyderabad, Telangana 500007, India

[‡]College of Science, Engineering and Health, Advanced Materials & Industrial Chemistry, School of Applied Sciences, RMIT University, GPO BOX 2476, Melbourne 3001, Australia

Ⓢ *Supporting Information*

ABSTRACT: Rare earth (RE = La, Pr, Nd, Gd and Sm) metal-doped Ni-Al (Ni-RE-Al) hydrotalcite precursors were obtained by coprecipitation and calcined to form mixed oxide catalysts. The physicochemical characteristics of calcined and reduced Ni-RE-Al samples were determined by X-ray powder diffraction, Brunauer−Emmett−Teller surface area, H_2 temperature-programmed reduction, O_2 pulse chemisorption, UV-diffuse reflectance spectroscopy, electron spin resonance spectrometry, and Fourier transform infrared spectroscopy. The catalysts were evaluated for CH_4 decomposition at 550 °C until their complete deactivation. The deactivated catalysts were examined by transmission electron, scanning electron, and Raman spectroscopy and elemental analysis. The Raman spectra indicated the presence of both ordered and disordered carbon in deactivated catalysts. A correlation is drawn between H_2 production rates and the Ni metal surface area of catalysts. The addition of La to Ni-Al dramatically changed the Ni behavior, leading to higher H_2 yields.

KEYWORDS: CO_x free H_2, Rare earth metals, CH_4 decomposition, Raman, Electron spin resonance, Carbon nanotubes
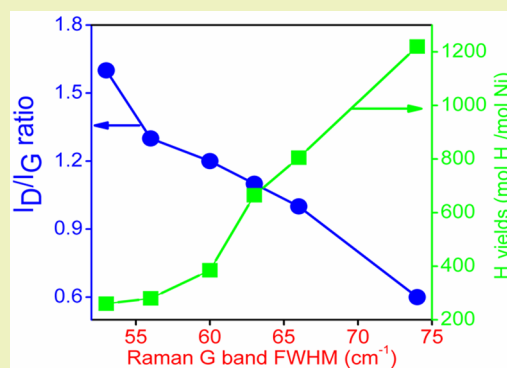
INTRODUCTION

Increasing environmental concerns has prompted a search for clean transportation fuels to avoid vehicular emissions like CO_x, NO_x, and SO_x. Recently, hydrogen has emerged as a clean alternative to fossil fuels without any emissions; thus, its market demand is increasing steadily.[1,2] On this basis, the production of hydrogen has drawn more attention from scientific as well as industrial sectors. Even though steam reforming of hydrocarbons has industrially been widely used to produce hydrogen, it has the disadvantage of higher CO_2 emissions and CO impurities in hydrogen. Hydrogen with CO impurities cannot be used directly in fuel cells, and the cost of the necessary separation has become exorbitant.[3] Catalytic decomposition of methane (CDM) (Scheme 1) is a favorable process for the production of pure hydrogen, which can be directly used in fuel cells as well as for several other applications.

$$CH_4 \rightarrow C + 2H_2; \; \Delta H° = 75.6 \text{ kJ mol}^{-1} \qquad (1)$$
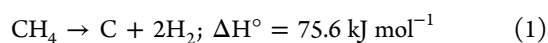
From an economical point of view, CDM is a useful technology because it produces not only pure H_2 but also stable valuable carbon nanotubes (CNTs) or carbon nanofibers (CNFs) rather than CO_2.[4−6] Compared to steam reforming, pure hydrogen can be obtained by the CDM process but has the disadvantage that catalyst deactivation occurs after a certain period. It has been reported that the catalyst deactivation depends on the reaction conditions, including temperature, feed flow, and so forth.[7] During the reaction, methane is adsorbed on the metal particle followed by decomposition and deposition of carbon on the metal surface. The deposited carbon diffuses toward the opposite face of the metal where it crystallizes in the form of carbon nano fibers/tubes. In general, the rate of carbon deposition is controlled by isothermal carbon diffusion through the metal particle, and the deactivation of the catalyst is explained by blocking of the active sites by carbon deposition.[8] The supported Ni, Fe, and Co catalysts are found to be effective for CDM,[9−14] and among these, Ni catalysts are active even at low temperatures. Studies on nickel-based catalysts are an important research area not only for CDM but also for CH_4 conversion to syngas. In earlier reports, modified Ni catalysts were explored at lower reaction temperatures, where they showed lower activity.[15,16] The addition of other metal to a Ni catalyst may increase CDM activity and also increase stability even at higher temperatures. Among the Cu-, Rh-, Pd-, Ir-, and Pt-doped Ni catalysts, Ni-Pd exhibited the best CDM activity through an alloying effect.[17] However, it has been observed in other studies
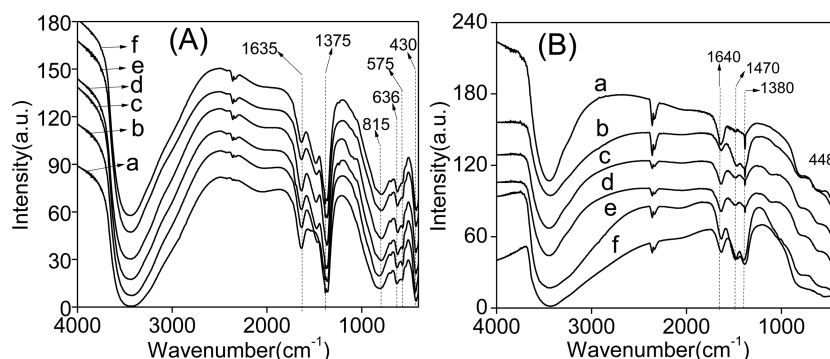
Figure 1. FT-IR spectra of (A) oven-dried and (B) calcined (a) Ni:Al (2:1), (b) Ni:La:Al (2:0.1:0.9), (c) Ni:Pr:Al (2:0.1:0.9), (d) Ni:Nd:Al (2:0.1:0.9), (e) Ni:Sm:Al (2:0.1:0.9), and (f) Ni:Gd:Al (2:0.1:0.9) samples.

that Cu-modified Ni catalysts demonstrated significantly better CDM rates.[18−23] Nevertheless, studies pertaining to stabilization of Ni by rare earth (RE) metals have not to date been investigated in detail. In recent years, layered double hydroxides (LDHs), anionic clays, and hydrotalcite (HT)-type materials, which belong to the same family, have gained importance due to their application as catalysts and catalytic precursors.[24] A molar ratio of $M^{2+}/(M^{2+} + M^{3+})$ in the range of 0.17−0.33 mainly determines the formation of HT-like compounds. In the present study, we have synthesized RE-doped Ni-Al hydrotalcite precursors by coprecipitation, which were subsequently decomposed in static air at 550 °C to produce mixed oxides. These mixed oxides were thoroughly characterized using X-ray diffraction (XRD), Brunauer−Emmett−Teller (BET) surface area, temperature-programmed reduction (TPR), O_2 pulse chemisorption, ultraviolet-diffuse reflectance spectroscopy (UV-DRS), electron spin resonance spectroscopy (ESR), and Fourier transform infrared spectroscopy (FT-IR). These oxides as catalysts were evaluated for CDM activity at 550 °C and atmospheric pressure until complete deactivation. The deactivated catalysts were investigated by transmission electron microscopy (TEM), scanning electron microscopy (SEM), Raman spectroscopy, and CHNS analysis.

EXPERIMENTAL SECTION

Preparation of Ni-RE-Al Hydrotalcite Precursors. The Ni-RE-Al precursors with a layered HT-like anionic clay structure were prepared by the coprecipitation method. Two solutions, namely, solution (A) containing the required amount of metal nitrates (Ni, RE, and Al in a 2:0.1:0.9 mol ratio) and solution (B) containing the precipitating agents (2 M NaOH and 1 M Na_2CO_3), were added slowly and simultaneously to a beaker containing distilled water while stirring and maintaining a constant pH of ∼9 at room temperature. The resulting precipitate was washed with distilled water several times until the pH of the washings reached the pH of distilled water. The precipitate was dried at 100 °C for 12 h and subsequently calcined in static air at 550 °C for 5 h.

Characterization of Catalysts. The XRD patterns of the samples were recorded on a Rigaku Miniflex X-ray diffractometer using Ni filtered Cu Kα radiation (λ = 1.5406 Å) from 2θ = 10−80° at a scan rate of 2°/min with a 30 kV beam voltage and a 15 mA beam current. The surface areas of the catalysts were measured by physical adsorption of N_2 at −196 °C in an Autosorb-I instrument (Quantachrome), and the specific surface area was calculated using the BET method. The SEM images of the fresh and used catalysts were recorded using a JEOL-JSM 5600 instrument. TEM images were taken using a JEOL JEM 2010 high-resolution transmission electron microscope to analyze the samples dispersed in a methanol solution and suspended on a Cu grid (400 mesh, 3.5 mm diameter). The Raman spectra of deactivated catalysts were recorded with a Horiba Jobin−Yvon lab ram HR spectrometer using a laser beam excitation of λ = 632.81 nm. O_2 pulse chemisorption

measurements were carried out in a quartz microreactor connected with gas chromatography (GC) and a thermal conductivity detector (TCD). Approximately 50 mg of catalyst was loaded in an isothermal zone of a quartz reactor (i.d. = 6 mm, length = 30 cm). Prior to being measured, the samples were reduced at 550 °C in a H_2 stream for 2 h. Then, the sample was cooled to 260 °C in helium gas, and gas flow continued at this temperature for 30 min. Then, the sample was titrated with 5.01% O_2 in helium at 260 °C. The O_2 uptake on a reduced Ni-RE-Al sample was calculated assuming the formation of a NiO phase upon oxygen chemisorption on metallic Ni.[25] The infrared spectra were recorded between 4000 and 400 cm^{-1} at room temperature using an Agilent Cary600 FT-IR spectrometer. The carbon analyses of deactivated catalysts were collected with a VARIO EL analyzer instrument. A Shimadzu UV-2000 spectrophotometer, equipped with a diffuse reflectance attachment with an integrating sphere containing $BaSO_4$ as a reference, was used to record UV−vis spectra at room temperature in the range of 190 and 800 nm with a sampling interval of 0.5 nm and slit width of 2 nm and converted to a Kubelka−Munk function. The ESR analysis of reduced Ni:RE:Al (2:0.1:0.9) samples were performed at room temperature using a JEOL/JES-FA200 spectrophotometer by X-band equipment with an operating frequency of υ = 9.029 GHz. The TPR analysis was carried out in a quartz microreactor connected to GC with TCD. Approximately 50 mg of catalyst was loaded in an isothermal zone of a quartz reactor (i.d. = 6 mm, length = 30 cm), degassed in 30 cc/min of helium gas, and heated at a rate of 10 °C/min to 300 °C by an electric furnace. After degassing, the sample was cooled to room temperature. Then, helium gas was switched to 5% H_2 in argon (30 cc/min), and the temperature was raised at 5 °C/min to 700 °C. Hydrogen consumption was measured by analyzing effluent gas by GC-TCD, and the H_2 uptakes were estimated with TPR of Ag_2O under a similar protocol.

Activity Measurements for CH_4 Decomposition. Prior to the reaction, ∼15−20 mg of catalyst sample was reduced at 550 °C at atmospheric pressure using 5% H_2 balanced Ar for 2 h in a fixed-bed vertical quartz reactor (i.d. = 1.0 cm, length = 46 cm) operated in a down flow mode. Methane (99.99%) was supplied by Bhuruka Gases, Ltd., and used without further purification. Catalytic decomposition of CH_4 (CDM) over Ni:RE:Al (2:0.1:0.9) catalysts were carried out at a reaction temperature of 550 °C and at a gas hourly space velocity (GHSV) of 180 h^{-1} until complete deactivation of catalyst (CH_4 conversion below 1%). The CH_4 conversion and H_2 formation were monitored at regular intervals using the online gas chromatograph (Varian CP-3800) with a carboxen column, TCD detector, and N_2 as a carrier gas.

RESULTS

FT-IR Analysis. FT-IR spectra of the oven-dried samples are shown in Figure 1(A). All samples showed a broad intense band between 3600 and 3000 cm^{-1} due to the OH stretching mode of layer hydroxyl groups of interlayer water molecules.[26] The position of this band should be dependent on the layer cation as

its electronegativity modified the electron density of the O−H bond (M−OH). However, the dependency is not distinguishable because of the extreme broadness of the band due to hydrogen bonding. The weak band at 1640−1620 cm^{-1} is due to the bending mode of water molecules. The sharp intense band at 1375−1365 cm^{-1} is due to mode ν_3 antisymmetric stretching of interlayer carbonate, which is shifted to a lower frequency compared to the free CO_3^{2-} band (due to strong hydrogen bonding of carbonate with hydroxyl sheets and H_2O molecules in the interlayer). The bands below 1000 cm^{-1} (~815 cm^{-1}) can be ascribed to mode ν_2 of carbonate and to M−OH modes. These results confirm the presence of carbonate, as well as the absence of nitrate, in the interlayer space of the rare earth metal-doped Ni-Al hydrotalcites. Formation of an OH-containing phase LDH (meixnerite) is very unlikely because of the known preferential intercalation of carbonate.[27] The FT-IR spectra of calcined samples are shown in Figure 1(B). The broad band observed at 3450−3660 cm^{-1} is ascribed to the presence of hydrogen bonded OH. The band situated at 1640 cm^{-1} is associated with the presence of HCO^{3-}. The band at ~448 cm^{-1} is the Ni-O stretching mode.[27] A weak band appearing at 1470 cm^{-1} is ascribed to the bridged-bidentate (i.e., carbonate) complexation of the interlayer in the LDHs.

X-ray Diffraction Analysis. The XRD spectra of oven-dried Ni:RE:Al (2:0.1:0.9 mol ratio) samples (Figure 2(A)) showed the crystallized HT-like anionic clay structure ($Ni_6Al_2(OH)_3(CO_3\cdot OH)\cdot 4H_2O$) from reflections observed at 2θ = 11.7°, 23.5°, 35.1°, 47.3°, and 62.6° [ICSD #15-0087].[24] The XRD spectra of the calcined samples (Figure 2(B)) revealed decomposition during calcination in air at 550 °C over 5 h by the emergence of a broad peak corresponding to NiO.[28] Neither Al_2O_3 nor any of the RE oxides are seen in these samples, which may be due to either proper mixing of these phases within the bulk mixture during the preparation and calcination or the crystal size of Al_2O_3 and/or the RE-oxides may be below the limit of X-ray detection. In calcined Ni:RE:Al (2:0.1:0.9 mol ratio) samples, the crystal domain size of NiO is determined by the Scherrer formula with respect to the NiO (111) plane (Table 1). This shows that the NiO domain size is varied by doping of the rare earth metals. The XRD patterns of reduced Ni:RE:Al (2:0.1:0.9 mol ratio) samples (Figure 2(C)) indicated only the metallic Ni phase with reflections at 2θ = 44.49°, 51.85°, and 76.38° [ICSD # 87-0712]. The crystallite size of nickel is increased after reduction in all of the samples except for Ni-Al (Table 1).

Temperature-Programmed Reduction. Reduction of NiO is reported at ~500 °C. The H_2-TPR profiles of calcined Ni:RE:Al samples (Figure 3) show T_{max} for Ni:Al, Ni:La:Al, Ni:Pr:Al, Ni:Nd:Al, Ni:Sm:Al, and Ni:Gd:Al of 495, 590, 545, 516, 546, and 558 °C, respectively. In general, a shift in the reduction maxima is influenced by metal and support interactions. T_{max} >500 °C in the case of the RE-doped Ni-Al samples is higher than the T_{max} of Ni-Al (~495 °C). The T_{max} of RE-doped Ni-Al being higher than that of Ni-Al is an indication of a strong interaction between nickel particles with RE:Al, which could effectively suppress the grain growth of the NiO phase (Table 1) and lead to increases in the catalytic activity. These results emphasize that the lanthanide additives have a strong influence on the metal−support interaction.[29,30]

BET-Surface Area and O$_2$ Pulse Chemisorption Measurements. The BET surface area of Ni:RE:Al calcined samples are reported in Table 2. Ni-Al (2:1) showed a slightly lower surface area (~120 m^2/g) than that of RE-doped Ni-Al. The Ni metal surface area of Ni:RE:Al (2:0.1:0.9) samples were
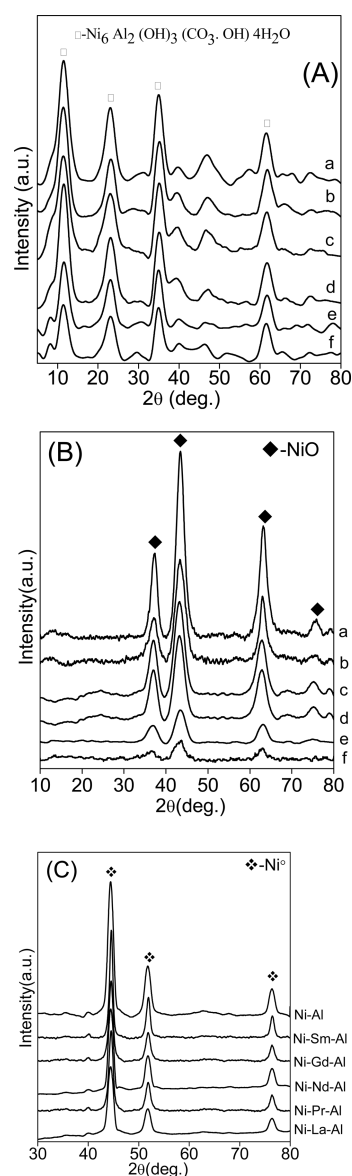

Figure 2. XRD patterns of (A) oven-dried, (B) calcined, and (C) reduced (a) Ni:Al (2:1), (b) Ni:La:Al (2:0.1:0.9), (c) Ni:Pr:Al (2:0.1:0.9), (d) Ni:Nd:Al (2:0.1:0.9), (e) Ni:Sm:Al (2:0.1:0.9), and (f) Ni:Gd:Al (2:0.1:0.9 mol ratio) catalysts.

Table 1. Physicochemical Properties of Ni:RE:Al Samples

catalysts (2:0.1:0.9 mol ratio)	NiO crystallite size^a (nm)	Ni domain size^b (nm)	H$_2$ uptake^c (μmol/g-cat)
Ni:Al	8.3	6.8	896
Ni:La:Al	5.5	7.8	1543
Ni:Pr:Al	5.2	10.5	1372
Ni:Nd:Al	4.8	11.9	1338
Ni:Sm:Al	3.6	14.9	1323
Ni:Gd:Al	3.2	5.9	1493

^{a}From calcined XRD samples using the Scherrer formula. ^{b}From reduced XRD samples. ^{c}From TPR analysis.

estimated by O$_2$ pulse chemisorption measurements and reported in Table 2. The Ni-Al sample exhibited ~21.3 m^2/g Ni metal surface area, whereas upon the addition RE metals to Ni-Al, it is slightly increased. The La-doped Ni-Al displayed a
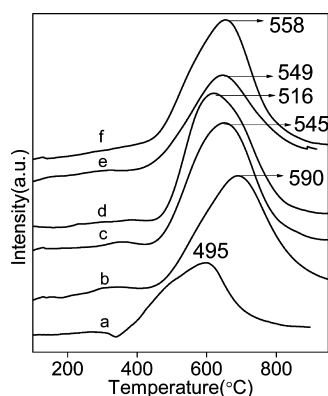
Figure 3. TPR profile of calcined (a) Ni:Al (2:1), (b) Ni:La:Al (2:0.1:0.9), (c) Ni:Pr:Al (2:0.1:0.9), (d) Ni:Nd:Al (2:0.1:0.9), (e) Ni:Sm:Al (2:0.1:0.9), and (f) Ni:Gd:Al (2:0.1:0.9 mol ratio) samples.

Table 2. O_2 Uptakes and Carbon Yields on Ni:RE:Al Catalysts

catalysts (2:0.1:0.9 mol ratio)	BET-SA (m²/g)	O_2 uptake (mmol/g-cat)	S_{Ni} (m²/g-cat)	carbon yield (gC/gNi)
Ni:Al	120	3.9	21.3	27
Ni:La:Al	135	5.9	32.4	125
Ni:Pr:Al	140	4.8	26.2	38
Ni:Nd:Al	142	4.5	24.4	29
Ni:Sm:Al	146	4.2	22.7	69
Ni:Gd:Al	148	4.0	21.6	83

higher Ni metal surface area than the other RE-doped Ni-Al samples.

Electron Spin Resonance Spectroscopy. Figure 4 represents the ESR spectra of reduced Ni:RE:Al samples. The
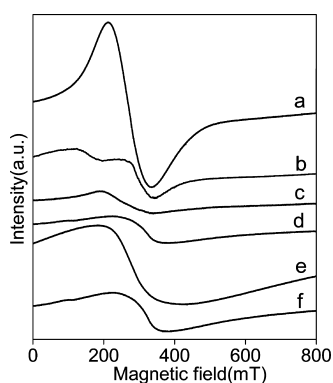

Figure 4. ESR spectra of (a) Ni:La:Al (2:0.1:0.9), (b) Ni:Al (2:1), (c) Ni:Pr:Al (2:0.1:0.9), (d) Ni:Nd:Al (2:0.1:0.9), (e) Ni:Sm:Al (2:0.1:0.9), and (f) Ni:Gd:Al (2:0.1:0.9 mol ratio) samples.

signal centered at g is equal to 2.2, which is attributed to metallic Ni.[31] The Ni-Al sample shows two anisotropic signals, one at lower and the other at a higher magnetic field. The lower magnetic field signal may be explained by spin−spin interactions. According to the Kawabata hypothesis, the broadening of the ESR signal of nanometal particles is affected by the quantum size effect and can be correlated to the size of the nanometal particle.[32] The following equation shows the relationship between the line width ΔH_{pp} (ΔH_{pp} = peak-to-peak width) of the ESR signal and the particle size of the nanoparticle.

$$d = a(\Delta H_{pp})^{0.5} \ldots\ldots\ldots \quad (2)$$

where d is the particle size in nm, ΔH_{pp} is the line width of the ESR signal in mT, and a is the proportionality constant. For nickel, a was previously determined to be 1.2.[33] The particle size of metallic Ni was investigated from the ESR spectra, and the results are presented in Table 3.

Table 3. Comparison of Ni Crystallite Size Measured from XRD and ESR Techniques

catalyst (2:0.1:0.9 mol ratio)	ESR particle size (nm)	XRD particle size (nm)	g values
Ni:Al	9.6	6.8	2.2
Ni:La:Al	12.2	7.8	2.2
Ni:Pr:Al	11.5	10.5	2.4
Ni:Nd:Al	14.6	11.9	2.08
Ni:Sm:Al	15.2	14.9	2.2
Ni:Gd:Al	13.7	5.9	2.02

Ultraviolet-Diffuse Reflectance Spectroscopy Analysis. The UV-DRS of oven-dried Ni:RE:Al (2:0.1:0.9 mol ratio) samples are shown in Figure 5(A). In the UV region, the samples showed a maximum absorption band around 200 nm. The bands observed in this region (200−300 nm) are ascribed to charge transfer processes. It is observed that all of the samples showed an absorption band around 650 nm, which corresponds to transition $3A_{2g} (F) \rightarrow 3T_{1g} (F)$ splits because of spin−orbit coupling, which is usually found at 710−650 nm. The band at 378 nm is due to $3A_{2g} (F) \rightarrow 3T_{1g} (P)$ transition.[27] The UV-DRS of calcined Ni:RE:Al (2:0.1:0.9 mol ratio) samples are shown in Figure 5(B). The absorption band position is determined by the first derivative of absorption bands. It can be seen that all of the catalysts exhibited a strong absorption band in the range of 240−290 nm because of charge transfer transitions from O_{2p} to metal. During doping of the lanthanides to Ni-Al, a strong and broad band grows in the UV region of 200−390 nm. Compared to Ni-Al (290 nm), the absorption bands of Ni:RE:Al samples are all blue-shifted. The samples showing an absorption band in the range of 241−250 nm is an indication of an interaction between Ni and RE-oxide species.[34] In contrast to fresh samples, the reduced catalysts showed two broad signals in the range of 200−430 nm (Figure 5(C)).

Catalytic Decomposition of Methane over Calcined Ni:RE:Al Catalysts. The methane decomposition activities are carried out at 550 °C and atmospheric pressure to determine the influence of the RE metal on CDM activity of Ni-Al catalysts (Figure 6). In general, Ni is known to be an active component for the thermal decomposition of methane, and Al_2O_3 support is an inactive material that plays a role in increasing the dispersion of the active component.[35] In time-on-stream analysis, all the catalysts showed higher initial conversion that decreased rapidly or gradually to some extent. The overall hydrogen yields over Ni:RE:Al catalysts at 550 °C are displayed in Figure 7. The H_2 yields are higher for the La-doped catalyst compared to other RE-doped catalysts. From this, it can be suggested that La can enhance methane decomposition activity of Ni-Al. Freni et al. have studied the Ni/MgO catalysts for steam reforming of ethanol and obtained higher H_2 yields with lower amounts of coke deposition on the catalyst surface[36]

Characterization of Deactivated Catalysts. *XRD Analysis of Deactivated Catalysts.* The XRD patterns of deactivated Ni:RE:Al (2:0.1:0.9 mol ratio) catalysts are shown in Figure 8. The reflections at $2\theta = 26.28°$, $45.2°$, $53.9°$, and $77.0°$ are attributed to graphitic carbon [ICSD # 01-0640], which are
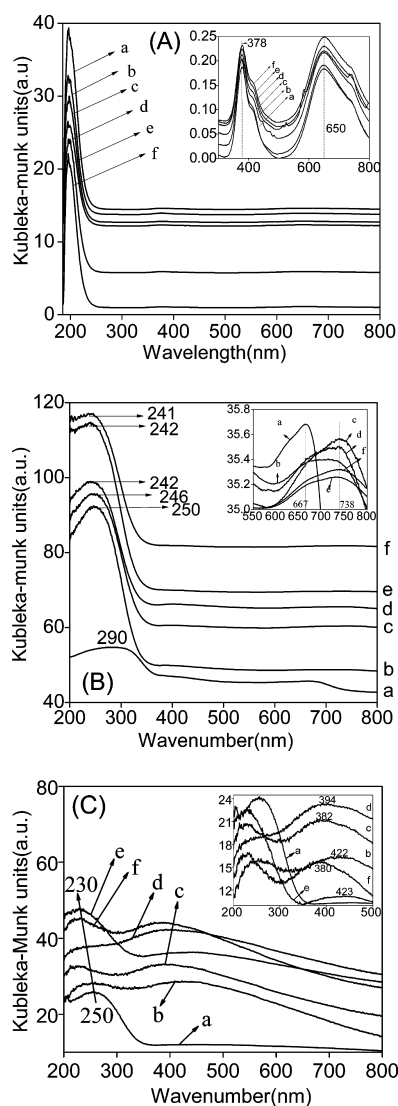
Figure 5. UV-DRS of (A) oven-dried, (B) calcined, and (C) reduced (a) Ni:Al (2:1), (b) Ni:La:Al (2:0.1:0.9), (c) Ni:Pr:Al (2:0.1:0.9), (d) Ni:Nd:Al (2:0.1:0.9 mol ratio) samples.
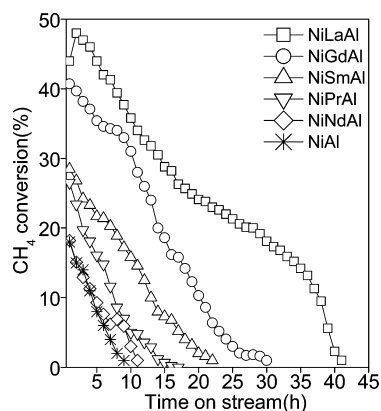
Figure 6. Methane conversions with time-on-stream until complete deactivation of the catalyst with a CH_4 flow rate = 30 mL min^{-1}, reaction temperature = 550 °C, and catalyst weight = ∼30 mg.

dominant compared to the lines at $2\theta = 44.4°$, 51.8°, and 76.4° due to the presence of metallic nickel [ICSD # 04-0850].[35]
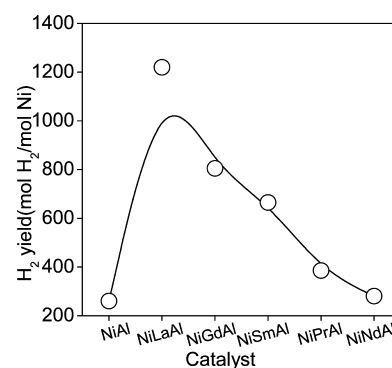
Figure 7. Hydrogen yields obtained during the CDM reaction over Ni:RE:Al (2:0.1:0.9 mol ratio) catalysts.
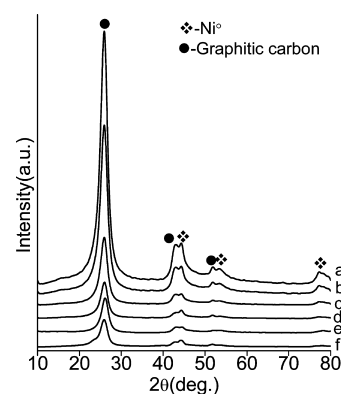
Figure 8. XRD patterns of deactivated (a) Ni:La:Al (2:0.1:0.9), (b) Ni:Gd:Al (2:0.1:0.9), (c) Ni:Sm:Al (2:0.1:0.9), (d) Ni:Pr:Al (2:0.1:0.9), (e) Ni:Nd:Al (2:0.1:0.9), and (f) Ni:Al (2:1 mol ratio) catalysts.

Raman Spectroscopic Analysis of Deactivated Catalysts. The nature of deposited carbon on deactivated Ni:RE:Al catalysts are confirmed by Raman spectra (Figure 9). The

Figure 9. Raman spectra of deactivated (a) Ni:Al (2:1), (b) Ni:La:Al (2:0.1:0.9), (c) Ni:Pr:Al (2:0.1:0.9), (d) Ni:Nd:Al (2:0.1:0.9), (e) Ni:Sm:Al (2:0.1:0.9), and (f) Ni:Gd:Al (2:0.1:0.9 mol ratio) catalysts.
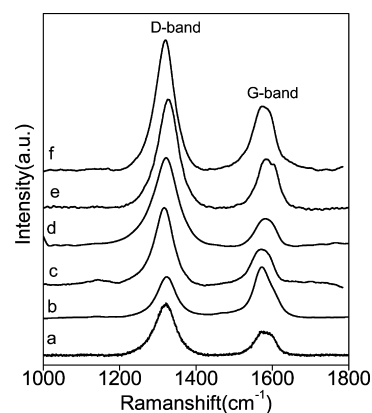
spectra displayed two distinct bands, one at around 1320 cm^{-1} (D-band) attributed to structural imperfection of graphite and/or amorphous carbon and the other around 1580 cm^{-1} (G-band) related to the in-plane carbon−carbon stretching vibrations rather than ordered structure carbon.[37,38] The degree of crystallinity of the deposited carbon can be obtained from the frequency and intensity of these bands. The ratio of the peak area

of the D band to that of the G band (I_D/I_G) is considered as an index for the crystalline order of graphite. The ratio (I_D/I_G) is inversely proportional to the average plane size of perfect graphenes.[39] A relationship between the I_D/I_G ratio and the full width at half-maximum (fwhm) is also reported for carbon nanofibers.[40] Figure 10 is a plot of fwhm of the G-band peak
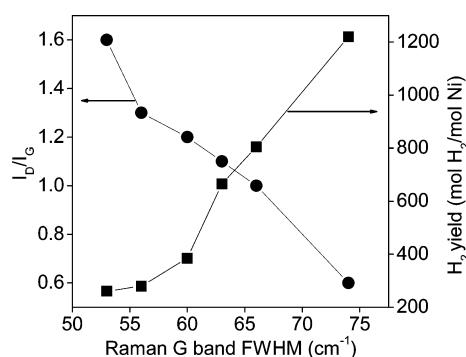

Figure 10. I_D/I_G ratio and carbon yields (mol H_2/mol Ni) as a function of fwhm of the G-band obtained from Raman spectra of deactivated catalysts.

against I_D/I_G ratios (calculated from Raman data) and carbon accumulation on the deactivated samples measured by CHNS analysis. It is observed that, with an increase in fwhm, the I_D/I_G ratio is decreased. Carbon accumulation against the G-bandwidth suggests the formation of highly ordered carbon over Ni:La:Al (2:0.1:0.9), where the I_D/I_G ratio is lower compared to other catalysts. The high CDM activity of Ni:La:Al (2:0.1:0.9) catalyst could possibly be due to deposition of a high amount of ordered carbon when compared to other catalysts. A measure of defect concentration in the graphenes can be obtained from I_D/I_G. The mean crystal domain size along the basal planes of deposited carbon is determined by applying Tuinstra and Koenig's law,[39] and the data is presented in Table 4.

Table 4. Raman Study of Deposited Carbon in Used Catalysts with the Intensity Ratio of Bands D and G and the Crystal Domain Size L_a

samples (2:0.1:0.9)	I_D/I_G	L_a (nm)
Ni:Al	1.6	7.04
Ni:La:Al	0.6	2.64
Ni:Pr:Al	1.2	5.28
Ni:Nd:Al	1.3	5.72
Ni:Sm:Al	1.1	4.84
Ni:Gd:Al	1.0	4.40

SEM and TEM Analysis of Deactivated Catalysts. Figure 11(A) shows the SEM images of deactivated (a) Ni:La:Al (2:0.1:0.9), (b) Ni:Sm:Al (2:0.1:0.9), and (c) Ni:Gd:Al (2:0.1:0.9) catalysts. The images clearly show that the deposited carbon is nanosized and has a few micrometers length of filamentous carbon.[12] The TEM image displayed in Figure 11(B) confirms this. The filament size is more or less the same as that of Ni at the tip of the carbon nanofiber.[7,40] These results are in good agreement with mechanisms proposed in the literature for filamentous carbon growth, which suggest that the diameter of carbon nanofibers must be approximately equal to the size of the Ni particle at the tip.[41,42]

DISCUSSION

The studies pertaining to methane decomposition to produce hydrogen over Ni-based catalysts, particularly rare earth metal-doped Ni-Al catalysts, and their physicochemical characteristics has been a topic of interest from a fundamental as well as an industrial point of view. The development of Ni-based catalysts is also an important area for the production of hydrogen by steam reforming ethanol. Frusteri et al.[43] have examined various noble and base metals supported on MgO and found that Ni/MgO exhibited superior performance in terms of ethanol conversion as well as lower carbon deposition compared to those of Pd/MgO systems. All of the samples showed CDM activity for a while and are completely deactivated. The cause of catalyst deactivation is well documented, and our earlier investigations also revealed possible reasons for deactivation of supported Ni catalysts during the CDM process.[9−12] It is attributed to the deposition of carbon on the catalyst surface/active sites and/or accumulated at the entrance of the pores leading to pore blockage. Nielsen and Trimm[44] reported that the carbon growth involves a gas phase reaction on the surface of the catalyst to form carbon, which eventually dissolves in the metal and would precipitate at a dislocation of the particle to form graphite. Among all of the catalysts, the Ni:La:Al (2:0.1:0.9) showed higher activity with an initial conversion of 43% with accumulation of 120 gC/gNi over a 42 h run. The high activity of Ni:La:Al is attributed some extent to a high Ni metal surface area (Table 2) and high reducing temperature (T_{max}) of NiO sites on Ni:La:Al (Figure 3). A shift in T_{max} to a high temperature is an indication of a strong interaction between Ni particles with the support. The reduction behavior of NiO is dramatically modified by the addition of rare earth metals to Ni-Al as demonstrated in TPR patterns of the Ni:RE:Al catalysts. The XPS analysis clearly indicated a shift of the Ni_{2p} signal toward lower BE in the case of Ni-La-Al (see Supporting Information), probably due to a strong interaction between Ni and La−Al. This is further confirmed by the TPR analysis as the T_{max} is found at 590 °C. According to Zhang et al, weakly interacted NiO reduces at lower temperatures (i.e., 500 °C).[45] The deposited carbon on deactivated catalysts is in the form of both ordered and disordered forms as seen from the Raman spectra. Further, the diffusion of deposited carbon occurs through the opposite face of the metal where they crystallize in the form of a continuous graphite structure. Such graphitic carbon formation between Ni and the support led to detachment of the Ni with support. In such situations, the catalysts that showed continuous activity exert growth of Ni at the tip of the carbon nanofiber or carbon nanotube as evidenced by the SEM and TEM analysis (Figure 11 (A and B)).[22] The SEM images showed the formation of carbon nanofibers (or nanotubes) on Ni:La:Al (2:0.1:0.9), Ni:Gd:Al (2:0.1:0.9), and Ni:Sm:Al (2:0.1:0.9) samples. XRD patterns of the deactivated catalysts clearly showed a sharp and strong diffraction line corresponding to graphitic carbon over the Ni:La:Al (2:0.1:0.9) sample. An increased Ni surface area is attributed to lanthanum oxide in a close proximity to nickel that could disperse the Ni metal crystallites as a result of the T_{max} being shifted to a higher temperature. The nature and growth of filamentous carbon depend on the Ni particle size and the quantity of nickel present at the catalyst surface as nickel particles that are too small do not form carbon filaments.[43] It was also reported that the sample is sustained for a longer period if the rate of diffusion of carbon through the nickel particle is higher than the rate of deposition of carbon on the surface of the Ni particle. If the reverse is true, the
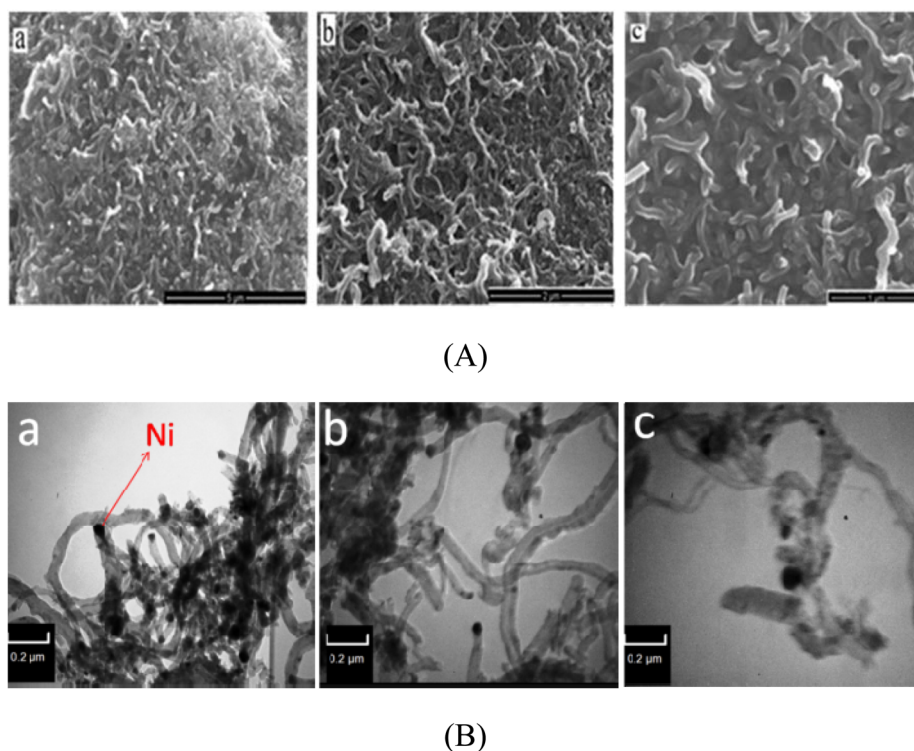
(A)

(B)

Figure 11. (A) SEM and (B) TEM images of deactivated (a) Ni:La:Al (2:0.1:0.9), (b) Ni:Sm:Al (2:0.1:0.9), and (c) Ni:Gd:Al (2:0.1:0.9 mol ratio) catalysts.

sample deactivates rapidly due to carbon deposition on the catalyst surface.[10] The deposition of carbon on the Ni surface may be curtailed by the presence of La in close proximity to the Ni particle as indicated by TPR analysis. As a result, growth of filamentous carbon may be increased, resulting in higher H_2 yields on the Ni-La-Al catalyst.

CONCLUSIONS

Rare earth metals-doped Ni-Al shows the formation of HT-like structures. Upon calcination, these materials decompose to form oxides. The Ni-RE-Al catalysts demonstrated better H_2 yields than Ni-Al. Doping of RE dramatically changed the behavior of Ni particles. The particle size of metallic Ni measured by ESR and XRD spectra is in close agreement. Higher H_2 yields on Ni-La-Al may be attributed to a large Ni surface area and also due to a strong interaction between Ni and RE-Al.

ASSOCIATED CONTENT

Ⓢ Supporting Information

Oven-dried catalysts characterized by TG/DTA, FT-IR spectra of reduced samples, XPS, and AAS analysis. The Supporting Information is available free of charge on the ACS Publications website at DOI: 10.1021/acssuschemeng.5b00372.

AUTHOR INFORMATION

Corresponding Author
*E-mail: akula@iict.res.in. Phone: +91-40-27191720/3510. Fax: +91-40-27160921.

Notes
The authors declare no competing financial interest.

REFERENCES
(1) Muradov, N. Z.; Veziroglu, T. N. From hydrocarbon to hydrogen-carbon to hydrogen economy. *Int. J. Hydrogen Energy* **2005**, *30*, 225−37.
(2) Hong, W.; Aik, C. L. Development of Metallic Nickel Nanoparticle Catalyst for the Decomposition of Methane into Hydrogen and Carbon Nanofibers. *J. Phys. Chem. C* **2012**, *116*, 26765−26775.
(3) Yi, S.; Aik, C. L. Synthesis of Ni and Ni-Cu supported on carbon nanotubes for hydrogen and carbon production by catalytic decomposition of methane. *Appl. Catal., B* **2015**, *164*, 61−69.
(4) Jong, K. P. D.; Geus, J. W. Carbon Nanofibers: Catalytic Synthesis and Applications. Carbon nanofibers: catalytic synthesis and applications. *Catal. Rev.* **2000**, *42*, 481−510.
(5) Dai, H.; Hafner, J. H.; Rinzler, A. G.; Colbert, D. T.; Smalley, R. E. Nanotubes as nanoprobes in scanning probe microscopy. *Nature* **1996**, *384*, 147−150.
(6) Dai, H.; Kong, J.; Zhou, C.; Franklin, N.; Tombler, T.; Fan, S. *Handbook of Nanophase and Nanostructured Materials*; Kluwer Academic/Plenum Publishers: New York, 2003; Vol. 4, pp 96−99.
(7) Suelves, I.; Lazaro, M. J.; Moliner, R.; Corbella, B. M.; Palacios, J. M. Hydrogen production by thermo catalytic decomposition of methane on Ni-based catalysts: influence of operating conditions on catalyst deactivation and carbon characteristics. *Int. J. Hydrogen Energy* **2005**, *30*, 1555−1567.
(8) Baker, R. T. K.; Barber, M. A.; Harris, P. S.; Feates, F. S.; Waite, R. J. Nucleation and growth of carbon deposits from the nickel catalyzed decomposition of acetylene. *J. Catal.* **1972**, *26*, 51−62.
(9) Ashok, J.; Naveen, K. S.; Venugopal, A.; Durga Kumari, V.; Subrahmanyam, M. CO_X-free H_2 production via catalytic decomposition of CH_4 over Ni supported on zeolite catalysts. *J. Power Sources* **2007**, *164*, 809−814.

(10) Ashok, J.; Naveen, K. S.; Subrahmanyam, M.; Venugopal, A. Production of CO_X Free Hydrogen by Catalytic Decomposition of Methane over Ni/HY Catalysts. *Catal. Lett.* **2007**, *118*, 139−145.

(11) Venugopal, A.; Naveen Kumar, S.; Ashok, J.; Hari Prasad, D.; Durga Kumari, V.; Prasad, K. B. S.; Subrahmanyam, M. Hydrogen production by catalytic decomposition of methane over Ni/SiO$_2$. *Int. J. Hydrogen Energy* **2007**, *32*, 1782−1788.

(12) Ashok, J.; Naveen, K. S.; Subrahmanyam, M.; Venugopal, A. Pure H$_2$ Production by Decomposition of Methane over Ni Supported on Hydroxyapatite Catalysts. *Catal. Lett.* **2008**, *121*, 283−290.

(13) Ermakova, M. A.; Ermakov, D. Y. Ni/SiO$_2$ and Fe/SiO$_2$ catalysts for production of hydrogen and filamentous carbon via methane decomposition. *Catal. Today* **2002**, *77*, 225−235.

(14) Li, X.; Zhang, Y.; Smith, K. J. Metal−support interaction effects on the growth of filamentous carbon over Co/SiO$_2$ catalysts. *Appl. Catal., A* **2004**, *264*, 81−91.

(15) Takenaka, S.; Shigeta, Y.; Otsuka, K. Supported Ni−Pd catalysts active for methane decomposition into hydrogen and carbon nanofibers. *Chem. Lett.* **2003**, *32*, 26−27.

(16) Chen, J.; Li, X.; Li, Y.; Qin, Y. Production of hydrogen and nanocarbon from direct decomposition of undiluted methane on high-nickel Ni−Cu−alumina catalysts. *Chem. Lett.* **2003**, *32*, 424−425.

(17) Takenaka, S.; Shigeta, Y.; Tanabe, E.; Otsuka, K. Methane decomposition into hydrogen and nanofibers over supported Pd−Ni catalysts. *J. Catal.* **2003**, *220*, 468−477.

(18) Reshetenko, T. V.; Avdeeva, L. B.; Ismagilov, Z. R.; Chuvilin, A. L.; Ushakov, V. A. Carbon capacious Ni-Cu-Al$_2$O$_3$ catalysts for high-temperature methane decomposition. *Appl. Catal., A* **2003**, *247*, 51−63.

(19) Li, Y.; Chen, J.; Qin, Y.; Chang, L. Simultaneous production of hydrogen and nanocarbon from decomposition of methane on a nickel-based catalyst. *Energy Fuels* **2000**, *14*, 1188−1194.

(20) Suelves, I.; Lazaro, M. J.; Moliner, R.; Echegoyen, Y.; Palacios, J. M. Characterization of NiAl and NiCuAl catalysts prepared by different methods for hydrogen production by thermo catalytic decomposition of methane. *Catal. Today* **2006**, *116*, 271−280.

(21) Echegoyen, Y.; Suelves, I.; Lazaro, M. J.; Moliner, R.; Palacios, J. M. Hydrogen production by thermocatalytic decomposition of methane over Ni-Al and Ni-Cu-Al catalysts: Effect of calcination temperature. *J. Power Sources* **2007**, *169*, 150−157.

(22) Lazaro, M. J.; Echegoyen, Y.; Suelves, I.; Palacios, J. M.; Moliner, R. Decomposition of methane over Ni-SiO$_2$ and Ni-Cu-SiO$_2$ catalysts: Effect of catalyst preparation method. *Appl. Catal., A* **2007**, *329*, 22−29.

(23) Pinilla, J. L.; Moliner, R.; Suelves, I.; Lazaro, M. J.; Echegoyen, Y.; Palacios, J. M. Production of hydrogen and carbon nanofibers by thermal decomposition of methane using metal catalysts in a fluidized bed reactor. *Int. J. Hydrogen Energy* **2007**, *32*, 4821−4829.

(24) Cavani, F.; Trifiro, F.; Vaccari, A. Hydrotalcite-type anionic clays: preparation, properties and applications. *Catal. Today* **1991**, *11*, 173−301.

(25) Stytsenko, V. D. Surface modified bimetallic catalysts: Preparation, characterization, and application. *Appl. Catal., A* **1995**, *126*, 1−26.

(26) Niranjan, B.; Lagnamayee, M.; Kulamani, P. Design and development of a visible light harvesting Ni−Zn/Cr−CO$_3^{2-}$-LDH system for hydrogen evolution. *J. Mater. Chem. A* **2013**, *1*, 4236−4243.

(27) Vicente, R.; Srinivasan, K. Layered double hydroxides with the hydrotalcite-typ structure containing Cu^{2+}, Ni^{2+} and Al^{3+}. *J. Mater. Chem.* **2000**, *10*, 489−495.

(28) Xiao, P. Y.; Wei, C.; Ning, W.; Fei, M. Hydrogen Production by Ethanol Steam Reforming on NiCuMgAl Catalysts Derived from Hydrotalcite-Like Precursors. *Catal. Lett.* **2011**, *141*, 1228−1236.

(29) Yuehua, C.; Huidong, Z.; Hengyong, X.; Wenzhao, L. On the nature of oxidic nickel phases in NiO/γ-Al$_2$O$_3$ catalysts. *Appl. Catal., A* **2007**, *331*, 60−69.

(30) Wei, W.; Chao, S.; Ran, R.; Zongping, S. A new Gd-promoted nickel catalyst for methane conversion to syngas and as an anode functional layer in a solid oxide fuel cell. *J. Power Sources* **2011**, *196*, 3855−3862.

(31) Selim, M. M.; Islam, H. A. E.M. Spectroscopic and catalytic characterization of Ni nano-size catalyst for edible oil hydrogenation. *Microporous Mesoporous Mater.* **2005**, *85*, 273−278.

(32) Kawabata, A. Electronic Properties of Fine Metallic Particles. III. E.S.R Absorption Line Shape. *J. Phys. Soc. Jpn.* **1970**, *29*, 902−904.

(33) Islam, H. A. E. M.; Hegazy, E. Z.; Kenawy, S.; Saleh, H. T. S. An Environmentally Benign, Highly Efficient Catalytic Reduction of *p*-Nitrophenol using a Nano-Sized Nickel Catalyst Supported on Silica-Alumina. *Adv. Synth. Catal.* **2010**, *352*, 1169−1178.

(34) Garbarino, G.; Campodonico, S.; Perez, A. R.; Carnasciali, M. M.; Riani, P.; Finocchio, E.; Busca, G. Spectroscopic characterization of Ni/Al$_2$O$_3$ catalytic materials for the steam reforming of Renewable. *Appl. Catal., A* **2013**, *452*, 163−173.

(35) Reshetenko, T. V.; Avdeeva, L. B.; Ismagilov, Z. R.; Chuvilin, A. L. Catalytic filamentous carbon as supports for nickel catalysts. *Carbon* **2004**, *42*, 143−148.

(36) Freni, S.; Cavallaro, S.; Mondello, N.; Spadaro, L.; Frusteri, F. Steam reforming of ethanol on Ni/MgO catalysts: H$_2$ production for MCFC. *J. Power Sources* **2002**, *108*, 53−57.

(37) Ashok, J.; Reddy, P. S.; Raju, G.; Subrahmanyam, M.; Venugopal, A. Catalytic Decomposition of Methane to Hydrogen and Carbon Nanofibers over Ni-Cu-SiO$_2$ Catalysts. *Energy Fuels* **2009**, *23*, 5−13.

(38) Ashok, J.; Raju, G.; Reddy, P. S.; Subrahmanyam, M.; Venugopal, A. Catalytic decomposition of CH$_4$ over NiO−Al$_2$O$_3$−SiO$_2$ catalysts: Influence of catalyst preparation conditions on the production of H$_2$. *Int. J. Hydrogen Energy* **2008**, *33* (18), 4809−4818.

(39) Dussault, L.; Dupin, J. C.; Guimon, C.; Monthioux, M.; Latorre, N.; Ubieto, T. Development of Ni−Cu−Mg−Al catalysts for the synthesis of carbon nanofibers by catalytic decomposition of methane. *J. Catal.* **2007**, *251*, 223−232.

(40) Alvarez, W. E.; Pompeo, F.; Herrera, J. E.; Balzano, L.; Resasco, D. Characterization of single-walled carbon nanotubes (SWNTs) produced by CO disproportionation on Co−Mo catalysts. *Chem. Mater.* **2002**, *14*, 1853−1858.

(41) Fenelonov, V. B.; Derevyankin, A. Y.; Okkel, L. G.; Avdeeva, L. B.; Zaikovskii, V. I.; Moroz, E. M. Structure and texture of filamentous carbons produced by methane decomposition on Ni and Ni−Cu catalysts. *Carbon* **1997**, *35*, 1129−1140.

(42) Baker, R. T. K.; Barber, M. A.; Harris, P. S.; Feates, F. S.; Waite, R. J. Nucleation and growth of carbon deposits from the nickel catalyzed decomposition of acetylene. *J. Catal.* **1972**, *26*, 51−62.

(43) Frusteri, F.; Freni, S.; Spadaro, L.; Chiodo, V.; Bonura, G.; Donato, S.; Cavallaro, S. H$_2$ production for MC fuel cell by steam reforming of ethanol over MgO supported Pd, Rh, Ni and Co catalysts. *Catal. Commun.* **2004**, *5*, 611−615.

(44) Nielsen, J. R.; Trimm, D. L. Mechanisms of carbon formation on nickel-containing catalysts. *J. Catal.* **1977**, *48*, 155−165.

(45) Zhang, J.; Xu, H.; Jin, X.; Ge, Q.; Li, W. Characterizations and activities of the nano-sized Ni/Al$_2$O$_3$ and Ni/La−Al$_2$O$_3$ catalysts for NH$_3$ decomposition. *Appl. Catal., A* **2005**, *290*, 87−96.